Journal of the American Association for Laboratory Animal Science
Copyright 2007
by the American Association for Laboratory Animal Science

Vol 46, No 5
September 2007
Pages 54–63

Multidetector Computed Tomographic Morphology of Ovaries in Cynomolgus Macaques (*Macaca fascicularis*)

Jeryl C Jones,[1,*] Susan E Appt,[2] J Daniel Bourland,[3] Patricia B Hoyer,[4] Thomas B Clarkson,[2] and Jay R Kaplan[2]

Macaques are important models for menopause and associated diseases in women. A sensitive, noninvasive technique for quantifying changes in ovarian morphology would facilitate longitudinal studies focused on the health-related sequelae of naturally occurring or experimentally induced alterations in ovarian structure and function. Multidetector computed tomography (MDCT) is a fast, non-invasive imaging technique that uses X-rays, multiple rows of detectors, and computers to generate detailed slice images of structures. The purpose of this study was to describe the utility of MDCT for reliably characterizing ovarian morphology in macaques. Five macaques were scanned using contrast-enhanced MDCT. The following characteristics were described: 1) appearance of ovaries and adjacent landmarks, 2) effects of varying technical protocols on ovarian image quality, 3) radiation doses delivered to the pelvic region during scanning, and 4) MDCT estimates of ovarian volume and antral follicle counts versus those measured directly in ovarian tissue. Ovaries were distinguishable in all MDCT scans and exhibited heterogeneous contrast enhancement. Antral follicles appeared as focal areas of nonenhancement. Ovarian image quality with 5 pediatric scanning protocols was sufficient for discriminating ovarian margins. Pelvic region radiation doses ranged from 0.5 to 0.7 rad. Antral follicles counted using MDCT ranged from 3 to 5 compared with 3 to 4 counted using histology. Ovarian volumes measured using MDCT ranged from 0.41 to 0.67 ml compared with 0.40 to 0.65 ml by water displacement. MDCT is a promising technique for measuring longitudinal changes in macaque ovarian morphology reliably and noninvasively.

Abbreviations: CTDI, computed tomographic dose index; MDCT, multidetector computed tomography; MPR, multiplanar reformatting; ROI, region of interest; TLD, thermoluminscent detector

Cynomolgus and rhesus macaques (*Macaca fascicularis*, *M. mulatta*) are important models for studies of menopause and related diseases in women.[1,3,8,9,12,13,15,16,26,30,32-34,39,44,49,51,53,54] Ovarian volume is an accurate predictor of menopausal status in both women and macaque monkeys.[5,20,25,27,44,46,47,63] For example, women having a mean volume of less than 3 ml respond poorly to ovulation induction.[37] Additional evidence suggests that ovarian volume is a more sensitive marker of ovarian function than serum follicle-stimulating hormone concentrations.[18]

A noninvasive imaging technique for accurately characterizing in vivo changes in ovarian volume would facilitate longitudinal studies of experimentally induced or natural menopause in macaque models. The standard methods for characterizing changes in ovarian morphology are either insufficiently repeatable in monkeys (for example, transabdominal ultrasonography) or destroy the tissue of interest (ovariectomy) and thus cannot be used for serial assessments.[3,16] Use of these methods therefore precludes longitudinal studies comparing changes in ovarian morphology with age, hormone levels, and application of experimental treatments.

In women, multidetector computed tomography (MDCT) has been established as a fast, noninvasive imaging technique for characterizing ovarian morphology.[7,22,36,38,45,52,55,57] MDCT uses X-rays, an array of multiple detectors, and advanced computer processing to generate high detail slice images of the body.[29] Advantages of MDCT include high-speed acquisition of data (whole-body scans with 0.5- to 1-mm thick slices can be completed in less than 30 s), low operator dependency, and the ability to repeatably visualize structures of interest without superimposition of overlying bone, gas, feces, or other obstacles. Transverse MDCT slice data can be stored and later used to create multiplanar reformatted (MPR) and three-dimensional volume-rendered images without having to repeat scans. Three-dimensional images can be rotated in space as needed to understand complex anatomic relationships. The density, area, and volume of individual structures can be calculated using hand-traced regions of interest in sequential slices or through the use of automated software.[36,38,41]

Contrast-enhanced CT has been validated as a reliable and accurate technique for estimating volumes of structures in experimental phantom studies and human case reports.[10,38,41,42] Low-radiation–dose MDCT protocols have been developed for use in human pediatric patients and have been found to provide good image quality.[14,23,28,61] The normal CT morphology of the human ovary and surrounding structures has been described.[7,22,50,52,57] To our knowledge, studies describing the use of MDCT for characterizing ovarian morphology in macaques are unavailable. The 4 objectives of this pilot study were to 1) describe the MDCT appearance of ovaries in adult macaques, 2) describe the effect of various pediatric MDCT protocols on ovar-

Received: 2 May 2007. Revision requested: 31 May 2007. Accepted: 15 Jun 2007.
[1]Department of Small Animal Clinical Sciences, Virginia-Maryland Regional College of Veterinary Medicine, Virginia Polytechnic and State University, Blacksburg, VA; [2]Wake Forest University Primate Center, Wake Forest University School of Medicine, Winston-Salem, NC; [3]Department of Radiation Oncology, Wake Forest University School of Medicine, Winston-Salem, NC; and [4]Department of Physiology, University of Arizona, Tucson, AZ.
[*]Corresponding author. Email: jcjones@vt.edu

Table 1. Scan parameters for MDCT protocols used in macaques 7409, 7232, and 7235

Protocol	1	2	3	4	5
Macaque no(s).	7409	7409	7409	7232, 7235	7232, 7235
kVp	80	80	80	80	80
mA	160	100	80	100	100
Acquisition	32 row, spiral	32 row, spiral	32 row, spiral	32 row, spiral	32 row, spiral
Algorithm	Detail	Detail	Detail	Detail	Detail
Slice thickness	0.5 mm	0.5 mm	0.5 mm	0.5 mm	1.0 mm
Rotation time	0.5 s	0.8 s	1.0 s	0.5 s	0.5 s
Scan field of view	18 cm	18 cm	18 cm	18 cm	18 cm
Display field of view	15.5 cm	15.5 cm	15.5 cm	15.5 cm	15.5 cm

All scans were initiated 10 s after bolus intravenous injection of 2 mg/kg nonionic, iodinated contrast medium.

ian image quality, 3) measure the radiation dose delivered to the ovarian region during MDCT scanning, and 4) compare MDCT ovarian morphology with gross and histologic morphology.

Materials and Methods

Animals. All procedures were done in accordance with federal, state, and institutional guidelines and were approved by the Institutional Animal Care and Use Committee of Wake Forest University. Five female cynomolgus macaques (*M. fascicularis*) were assessed. Three of these monkeys (nos. 7232, 7235, and 7409) were young adults (that is, approximately 5 y of age) at the time of scanning, whereas the other 2 (nos. 6980 and 6234) were aged (approximately 10 and 16 y, respectively). All animals were acquired from commercial sources. Four of the animals (7232, 7235, 6980, and 6234) had undergone a unilateral ovariectomy during a previous study, and the remaining monkey (7409) had both ovaries present at the time of scanning.

All monkeys were fed an isoflavone-free, semipurified diet prepared in our laboratory. This diet was designed to minimize potential confounders due to biologically active phytochemicals that are present in standard monkey chow.[60] The diet contained 20% of calories as protein (derived from casein, lactalbumin, and wheat flour), 30% of calories as fat (a mixture of saturated and unsaturated fats plant and animal fats), and 50% of calories as carbohydrates (dextrin, sucrose, and wheat flour). Vitamin mixture (AIN-93-VX, Harlan Teklad, Madison, WI) and mineral mixture (AIN-93-MX, Harlan Teklad) also were added to the diet. Animals were provided with 120 cal of diet per kilogram body weight, an amount that allows for wastage, in a social setting. Body weights were 3.3 kg for monkey 6980, 3.3 kg for 7409, 4.3 kg for 6234, 4.9 kg for 7232, and 4.9 kg for 7235.

MDCT anatomic landmarks for localizing ovaries. Whole-body MDCT scans from monkeys 6234, 6980, and 7409 were evaluated retrospectively. These scans had originally been used for a research project on cardiovascular disease. Postcontrast scans had been acquired either during or 5 to 10 min after CT angiography procedures. Scans for macaque 6234 had been performed with a 16-slice MDCT scanner (Lightspeed, General Electric Healthcare, Piscataway, NJ), and scans for macaques 6980 and 7409 had been performed with a 32-slice MDCT scanner (Aquilion 32, Toshiba America Medical Systems, Tustin, CA). Transverse, MPR, and 3-dimensional volume-rendered views of the ovaries were generated and reviewed by 2 observers (JJ, SA) using an image analysis workstation (Advantage Workstation, version 4.2, General Electric Healthcare). Anatomic features of the ovaries and adjacent landmarks were described by using a macaque anatomic atlas and human CT anatomy articles as references.[7,22,50,52,57,62]

Effect of varying MDCT scan protocols on ovarian image quality. New scans of the pelvic region of macaque 7409 were acquired by using a 32-slice MDCT scanner and 3 scanning protocols adapted from those used for human pediatric patients (protocols 1 through 3 in Table 1).[14,23,28,61] Protocols were preprogrammed for sequential execution by using the MDCT scanner's operator workstation. Each monkey was sedated inside a transport cage, by using ketamine (15 mg/kg) intramuscularly. Once loss of righting reflex was achieved, the animal was positioned supine on the CT table with the legs extended. A 26-gauge butterfly catheter was placed into the saphenous vein and taped into place. Vertical and horizontal pilot scans were created. Boundaries for the scan field of view included the cranial margins of the ilial wings and caudal margins of the tuber ischii. The lateral boundaries of the display field of view included the lateral margins of the ilial wings.

Iodinated, nonionic contrast medium (Iopromide, 300 mg I/ml, 2 ml/kg, Ultravist, Berlex, Montville, NJ) was administered through the butterfly catheter by rapid manual bolus. After a 10-s delay, the 3 preprogrammed protocols were performed sequentially.[24] Image data from each scan were archived to DVDs as DICOM files. Data were imported from DVDs to a laptop computer (PowerPC G4, Apple, Cupertino, CA) and reviewed by a single observer (JJ) using open-source DICOM image analysis software (OsiriX version 2.6 Medical Imaging Software, Los Angeles, CA). The orthogonal MPR tool was used to generate transverse, sagittal, and dorsal (coronal) planar views and to localize each ovary. The image was magnified 300%. The display window width was set at 200 HU and the window level was set at 95 HU. Ovarian image quality for each scan protocol was graded as excellent, good, fair, or poor.[28] Grades were assigned based on the observer's ability to discriminate ovarian margins from adnexa and to detect antral follicles (defined as focal areas of nonenhancement within the ovarian parenchyma). For each ovary during each protocol, the standard deviation of the CT number was used as a measure of image noise.[66] The CT number was calculated by using an oval region of interest (ROI) placed within the midslice image of the ovary. The ROI was placed such that it did not include an antral follicle.

Radiation doses delivered to the ovarian region during MDCT scanning. Scans of macaques 7232 and 7235 were acquired by using the same 32-slice MDCT scanner as that used in the previous experiment and 2 new pediatric protocols (protocols 4 and 5 in Table 1). The MDCT computer's estimated CT dose index (CTDI) was recorded for each protocol, after the boundaries for the scan fields of view were set (Figure 1).[14,19,58] A thermoluminescent detector (TLD) was placed on the ventral surface of each macaque's abdomen prior to initiating the 2 scanning protocols, and cumulative dose estimates (rad) were measured by using a commercial TLD reader (Harshaw TLD Model 5500 Automatic Reader, Thermo Fisher Scientific, Franklin, MA).

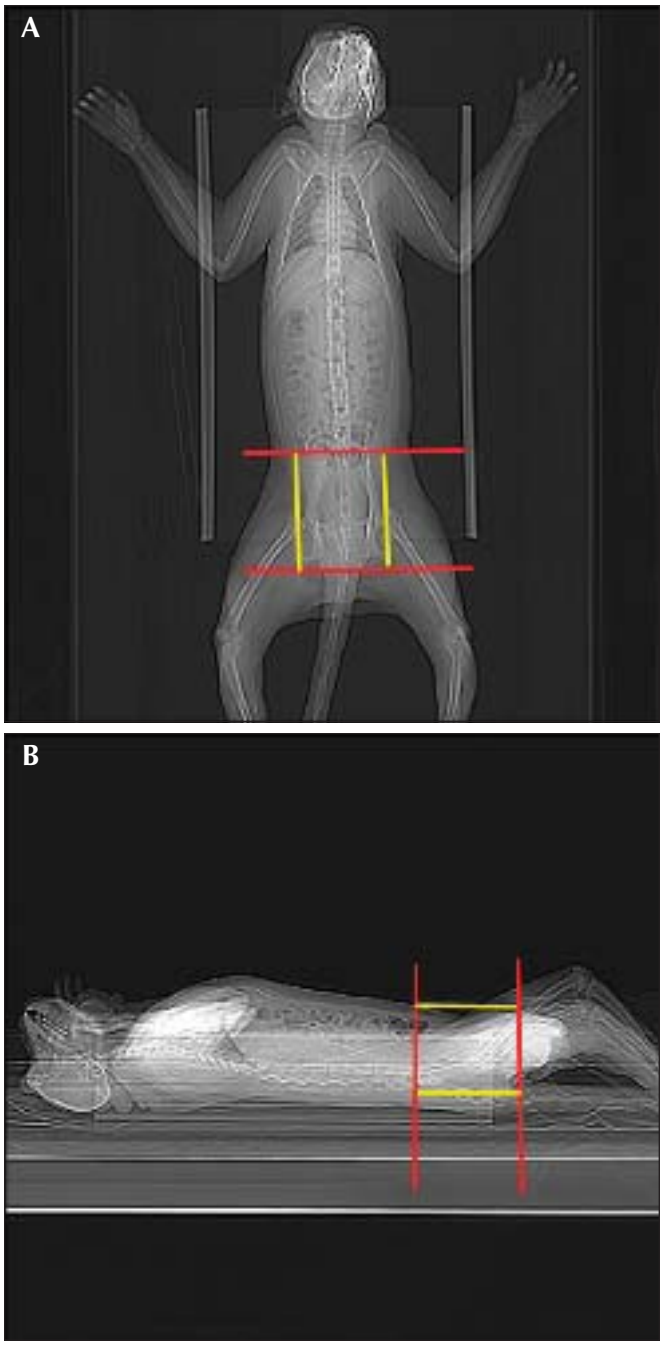

Figure 1. (A) Dorsoventral and (B) lateral pilot CT images demonstrating the positioning, scan field, and display field used for MDCT scanning and calculation of CTDI in macaque 7232. Boundaries for the scan field included the cranial margins of the ilial wings and the caudal margins of the tuber ishii (red). Boundaries for the display field included the lateral margins of the ilial wings, ventral abdominal wall, and dorsal margin of the ilial wings (yellow).

Figure 2. Photo demonstrating water displacement volume calculation for the trimmed ovary in macaque 7235. Volume was calculated as the difference in water levels before versus after placement of the ovary in the graduated cylinder.

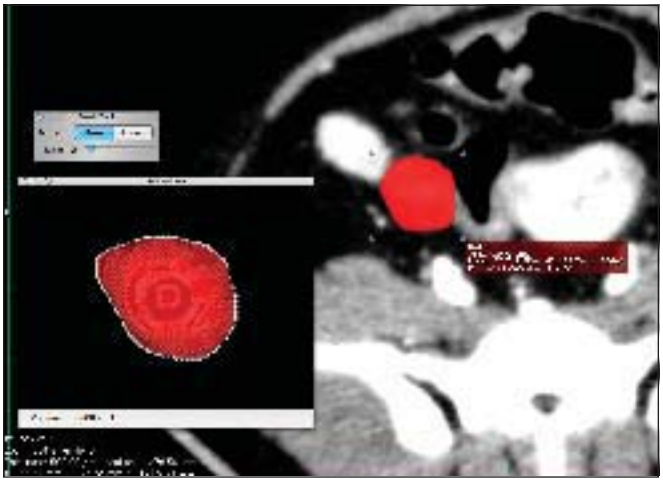

Figure 3. Computer monitor display demonstrating MDCT volume calculation for the right ovary in macaque 7232. The image is magnified 300%, the window width is set at 200 HU, and the window level is set at 95 HU. The hand-traced ovary ROI (red) is in the center of the display. The inset box to the left of the ovary displays a 3-dimensional summation image of all the traced ROIs and the calculated ovarian volume in cubic centimeters (0.6608 cm^3).

Comparison between MDCT, gross, and histologic morphology. Immediately after MDCT scanning, macaques 7232 and 7235 were euthanized by using pentobarbital (100 mg/kg intravenously). Complete necropsy examinations were done on each. The ovaries were removed and measured twice for actual ovarian volume by using a water displacement test: 1) the volume of the ovary with adnexa (fat, partial fallopian tube, and fimbria); and 2) the volume of the ovary alone, after the adnexa had been removed.[10] For this test, a graduated cylinder was filled with 8 to 20 ml of water (Figure 2). The water level was recorded prior to introduction of ovarian tissue. The ovary, with adnexa attached, then was placed in the graduated cylinder, and the total volume was recorded. The ovary was removed from the water, and adnexa was dissected away carefully. The volumes of water before and after introduction of ovarian tissue again were recorded. The volume of the ovary (with and without adnexa) was calculated by subtracting the volume of the water alone from the volume of the water containing the ovary (with

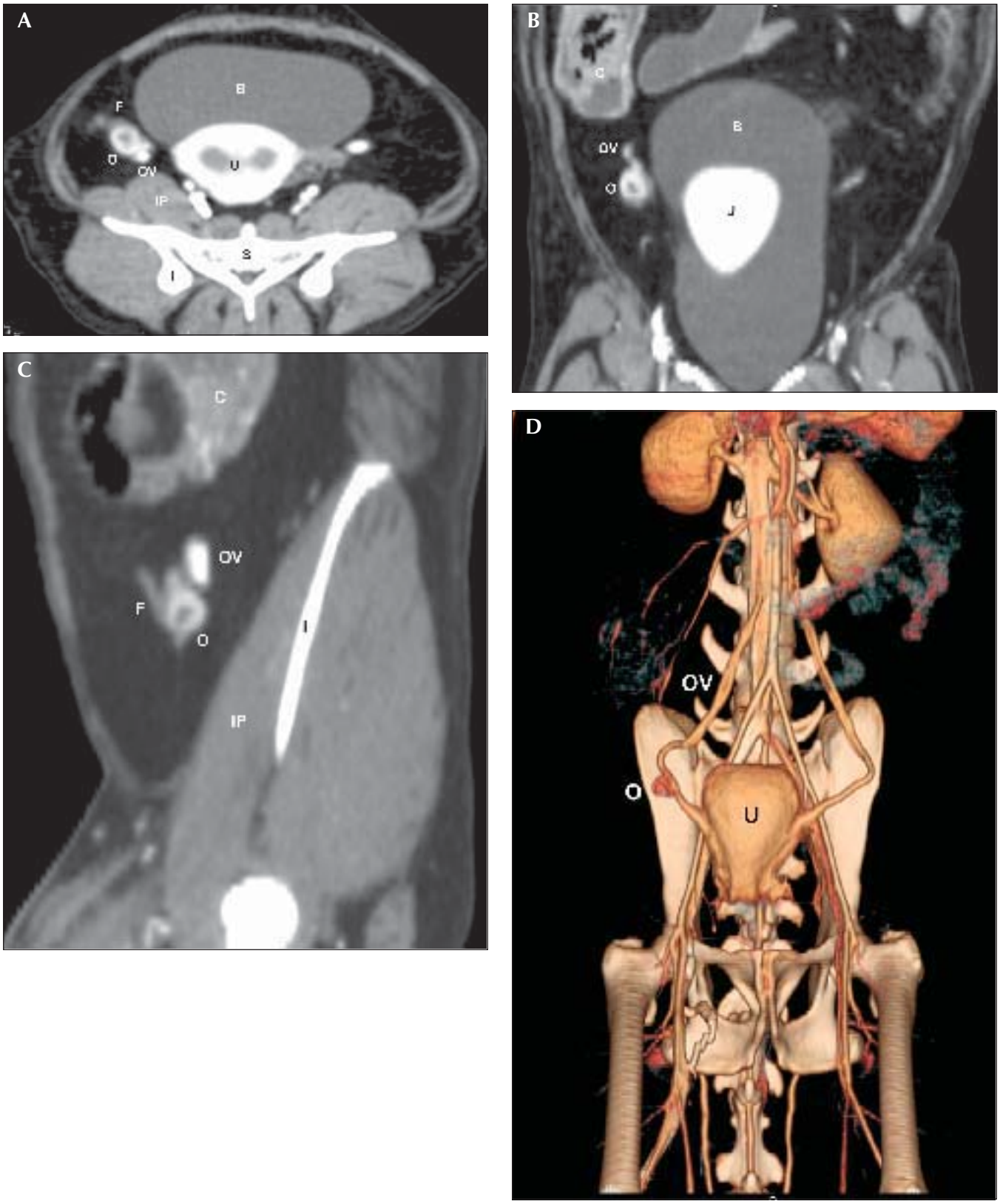

Figure 4. Contrast-enhanced (A) transverse, (B) dorsal, (C) sagittal, and (D) volume-rendered 3-dimensional CT images demonstrating the right ovary in macaque 6234 relative to adjacent anatomic landmarks. B, urinary bladder; F, fallopian tube; I, ilial wing; IP, iliopsoas muscle; O, ovary; OV, ovarian vein; S, sacrum; U = uterus.

and without adnexa).

After volume measurements, the ovaries were placed in Bouin fixative for 24 h before being transferred to 70% ethanol. They then were halved, embedded in paraffin, and shipped to The University of Arizona, where they were sectioned serially (every 4 to 5 µm) and stained with hematoxylin and eosin. Follicles in each ovary were classified and counted by a single observer who was unaware of MDCT findings. Follicles were classified

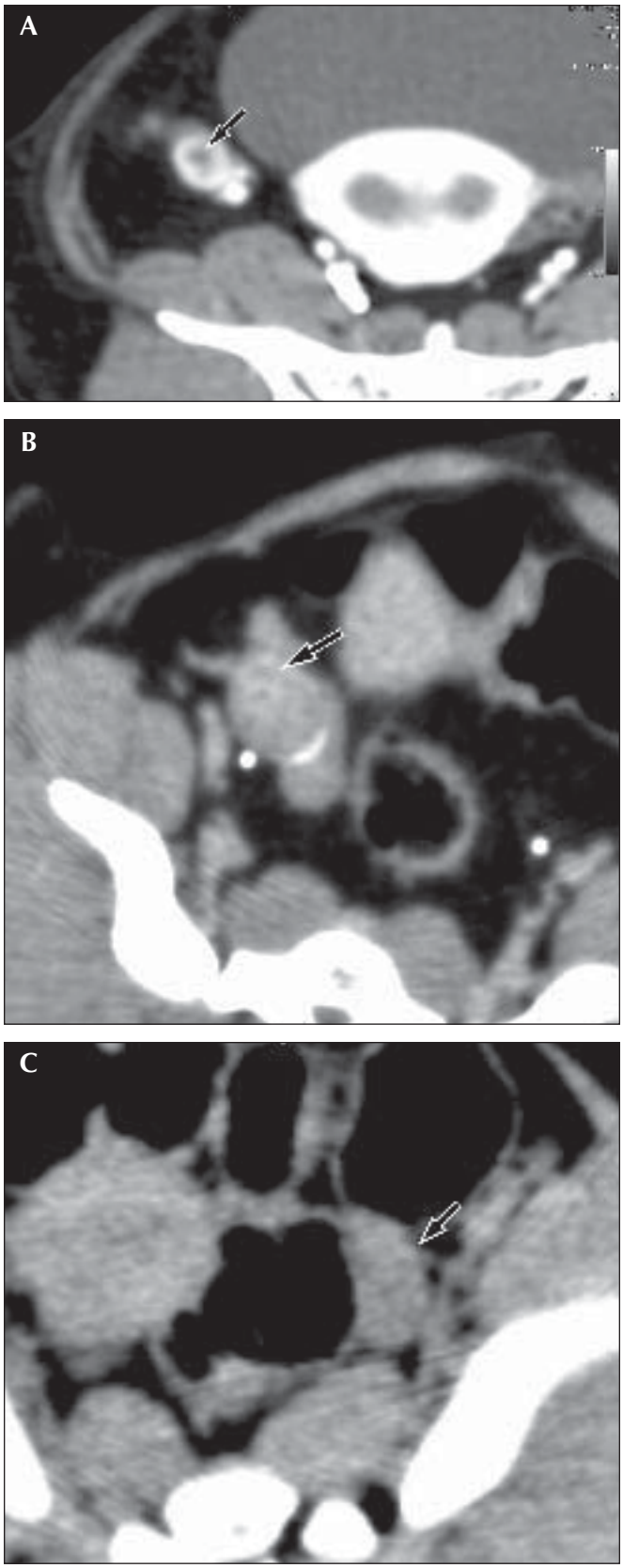

Figure 5. Transverse CT images demonstrating the effect of contrast-enhancement on the appearance of the right ovary in 3 macaques. (A) Macaque 6234. The ovary is markedly enhanced. Ovarian and antral follicle margins are easily visualized (arrow). (B) Macaque 6980. The ovary is mildly enhanced. Ovarian margins and at least two follicles are faintly visible (arrow). (C) Macaque 7409. The ovary is not contrast-enhanced. Ovarian margins and follicles are not distinguishable (arrow).

as primordial (oocytes surrounded by a single layer of flattened granulosa cells), primary (oocyte surrounded by a single layer of cuboidal cells), secondary (oocytes surrounded by 2 or more layers of cuboidal granulosa cells), and antral follicles (follicles containing a fluid-filled antrum). Antral follicles were counted every 100th section to avoid double counting of small preantral follicles. The total number of sections per ovary varied from 11 to 17 according to interindividual differences in ovarian size and the presence or absence of corpora lutea.[21,40,48]

Digital image data from MDCT scans were reviewed by a single observer (JJ), using the same computer, software, and MPR tools as for the previous image quality experiment. The observer was blinded to the necropsy measurements prior to generating and recording the MDCT measurements. Ovaries were displayed by using 300% magnification. An oval ROI was placed in the midslice location of the ovary to measure the mean CT density (in Hounsfield units). The display window width was set at 200 HU, and the window level was set at the mean CT density value. Transverse, sagittal, and dorsal planar views of each ovary were generated with the orthogonal MPR tool, and the number of antral follicles (focal areas of nonenhancement within the ovarian boundaries) was recorded. A point tool was used to mark the locations of follicles in order to avoid repeat counts. The ovarian area was hand-traced in sequential transverse slices by using the draw and erase functions of the ROI brush tool. After all slices had been traced, the volume of the selected ROI (Figure 3) was computed by using volume calculation software (OsiriX version 2.6 Medical Imaging Software, Los Angeles, CA). Volume measurements were performed 3 times for each scan, and average values were recorded.

Results

MDCT anatomic landmarks for localizing ovaries. Ovaries were visualized consistently in MDCT scans, and characteristics were similar to those described in women.[57] The localizing technique involved identifying the large cervix and uterus in the caudal (inferior) pelvic canal and then scrolling cranially (superior) through the transverse slices until the tortuous fallopian tubes could be seen exiting the lateral margins of the uterus. Orthogonal MPR images were helpful for differentiating ovaries from adjacent bowel (Figure 4). Volume-rendered 3D images were clearest when ovaries and blood vessels were at peak contrast enhancement. In such scans, the relationships between the ovaries, uterus, skeletal structures, ureters, and blood vessels could be observed readily from various viewing angles. In all scans, ovaries appeared as oval to lobular soft tissue structures partially enclosed by the lateral extremity and fimbria of each associated fallopian tube. The ovaries were positioned cranial or lateral to the uterus and ventral to the ureter and ovarian vein. Precontrast ovarian CT density values ranged from 19 to 73 Hounsfield units. Ovarian margins were calcified partially in macaque 6980. The margins of the ovaries and antral follicles were best distinguished from adjacent soft tissues in scans with contrast enhancement (Figure 5). In these scans, antral follicles could be discriminated as focal nonenhancing areas within the ovarian parenchyma. Preantral follicles were not visible in any of the scans.

Effect of varying MDCT scan protocols on ovarian image quality. Image quality was sufficient for discriminating ovarian margins and antral follicles in all 3 contrast-enhanced, pediatric MDCT protocols (Table 2; Figure 6). Ovarian margins were less distinct for both ovaries in scans performed with protocol 3 compared with protocols 1 and 2. Image noise (based on the standard deviation of the CT number) ranged from 11 to 24 Hounsfield units for the 3 protocols. Increasing ureteral or

Table 2. Image quality of 3 pediatric MDCT protocols in macaque 7409

Ovary	Parameter	Protocol 1	Protocol 2	Protocol 3
Right	Margin distinction	Good	Good	Fair
	Antral follicle distinction	Good	Good	Good
	Image noise[a]	24	24	24
Left	Margin distinction	Good	Good	Fair
	Antral follicle distinction	Good	Fair	Good
	Image noise	17	16	11

[a]CT number standard deviation measured at the ovary mid-slice (Hounsfield units).

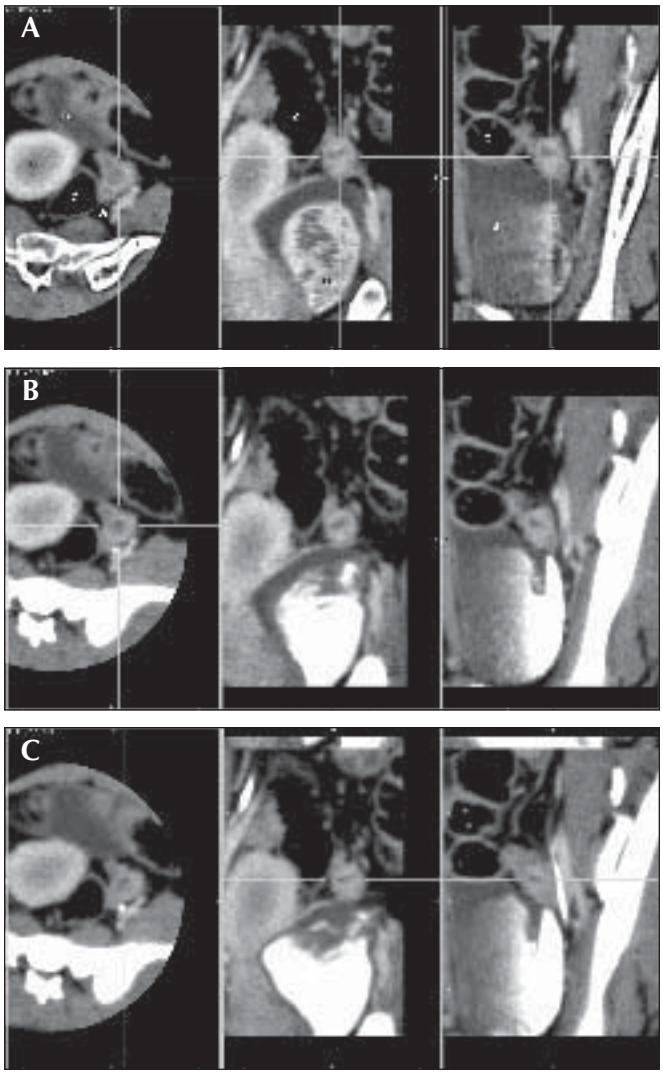

Figure 6. MPR CT images demonstrating the effect of varying MDCT scan protocols on the appearance of the left ovary and adjacent anatomic structures in macaque 7409. See Table 1 for protocol descriptions in detail. (A) Protocol 1: good discrimination of ovary margins versus adnexa and good visualization of antral follicle. (B) Protocol 2: good discrimination of margins, and fair visualization of follicle. (C) Protocol 3: fair discrimination of margins, good visualization of follicle. Window width, 200 HU; window level, 95 HU. B, urinary bladder (some partial volume averaging with rectum noted in dorsal planar view); C, colon; I, ilium; U, uterus; Ur, ureter.

urinary bladder contrast enhancement was noted in sequential scans, as was the presence of streak artifacts, some of which seemed to arise from the surrounding pelvic bones, and some from a metallic object in the nearby colon (Figure 7). The source of this metallic object was unknown. Retrospective review of

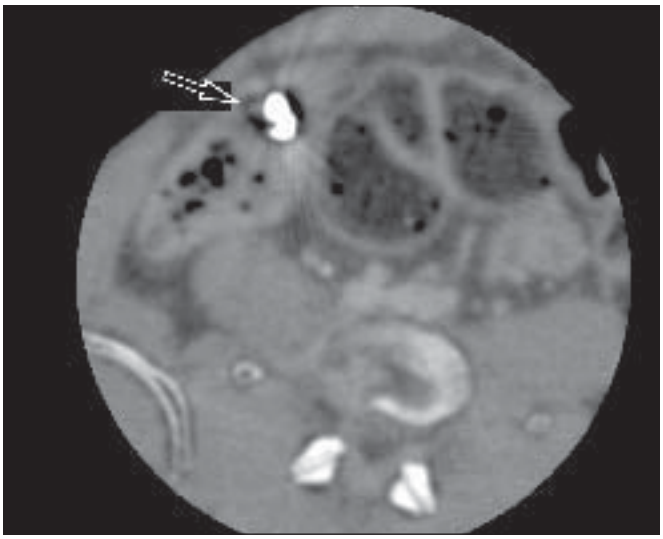

Figure 7. Transverse CT image demonstrating streak artifacts radiating from a metallic object (arrow) in the lumen of the colon in macaque 7409.

CT images from a scan performed 1 mo earlier did not reveal any metallic objects in this macaque.

Radiation doses delivered to the ovarian region during MDCT scanning. Corrected CTDI radiation doses were similar for pediatric MDCT scans obtained with 1-mm slice thickness (protocol 5, 0.46 rad) versus the scans obtained with 0.5-mm slice thickness (protocol 4, 0.51 rad; Table 3). Radiation doses measured for both scans with TLD ranged from 0.79 to 0.85 rad, with a mean of 0.82 rad. The readings were energy-corrected (factor of 1.25) for the over-response of the TLD at lower photon energies to a mean of 0.66 rad.

Comparison between MDCT, gross, and histologic morphology. Focal nonenhancing regions in MDCT images of the ovaries were confirmed as antral follicles on histology (Figure 8). Histologic total follicle counts ranged from 1503 to 2231 (Table 4). Antral follicle counts from MDCT scans ranged from 3 to 5, and histologic antral follicle counts ranged from 3 to 4. Volume estimates from MDCT scans ranged from 0.41 to 0.67 ml, actual volumes for untrimmed ovaries ranged from 0.60 to 1.5 ml, and actual volumes for trimmed ovaries ranged from 0.40 to 0.65 ml (Table 5). In 3 of the 4 scans, MDCT estimates of ovarian volume were within 0.01 to 0.02 ml of trimmed actual ovarian volumes. In 1 scan, acquired by using 0.5-mm slice thickness, the MDCT volume estimate was 0.14 ml greater than the actual trimmed volume. This difference was primarily due to difficulties in distinguishing the cranial and caudal ovarian margins from adnexa.

Discussion

In this study, MDCT enabled consistent identification of the ovaries and surrounding structures, with an appearance

Table 3. Average radiation doses measured using two MDCT scanning protocols in macaques 7232 and 7235

	Protocol 4	Protocol 5
CTDI, uncorrected (16 cm diameter)	0.5 rad	0.5 rad
CTDI, corrected (10 cm diameter)	0.6 rad	0.6 rad
TLD measurement	not available	0.7 rad
Dose assessment	0.6 rad	0.6 rad

CTDI, computed tomographic dose index (calculated by CT computer for each scan); TLD, thermoluminescent detector (measurement of average dose delivered to ovarian region for both sequential scans).

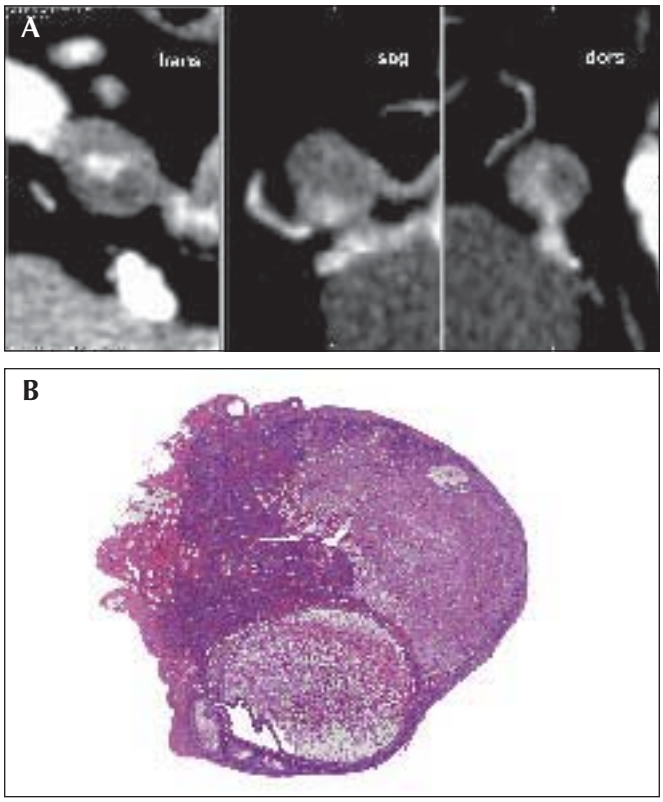

Figure 8. (A) MPR MDCT versus (B) histology slice images of the right ovary and a large antral follicle in macaque 7232. The maximal diameter of the follicle measured 4.42 mm. trans, transverse; sag, sagital; dors, dorsal.

comparable to that reported for women.[57] Importantly, ovarian volume estimates from MDCT scans closely matched values measured from water displacement examinations, suggesting that the MDCT technique can be used for noninvasive serial assessment of changes of ovarian volume.

Among other findings, contrast enhancement seemed necessary to distinguish ovarian and antral follicle margins, an observation consistent with previous studies in which the detection accuracy for small, soft tissue lesions was affected markedly by the degree of density change between the lesion and background tissue.[31,64] The presence of overlying bone or gas- or feces-filled bowel loops was not an impediment to visualizing ovaries with MDCT. This technique therefore provides an advantage over transabdominal ultrasonography, in which overlying bone or feces- or gas-filled bowel can cause inconsistent visualization of reproductive structures.[17] A transvaginal ultrasound approach can be used in women to help overcome this problem.[43] However, physical constraints make the use of transvaginal ultrasound impractical in most monkey species. Moreover, MDCT provides data that can be stored and reanalyzed as needed for future morphology studies of other pelvic structures, such as spine, pelvic bone, arteries and veins, uterus, cervix, urinary bladder, colon, rectum, and ureters.

Image quality was evaluated by using 3 MDCT protocols in a single subject. Scanning protocol parameters were adapted from those previously published for use in neonatal human patients.[14,23,28,61] Our goal was to develop a scanning protocol for future longitudinal studies that would keep the radiation dose as low as reasonably achievable while maintaining good image quality. In this image quality test, we standardized the kVp setting (80) and slice thickness (0.5 mm) while varying the mA settings (160 to 100 to 80) and rotation times (0.5 to 1.0 s). We also limited the boundaries of the scan and display fields of view to include only the pelvic region (that is, we targeted this region). To minimize the effect of image display factors on our comparisons, we used a constant image display window width of 200 HU and a window level of 95 HU. A previous study using cylindrical and spherical phantoms demonstrated that observer perception of margins is affected markedly by window display settings.[6]

We used a delay time of 10 s between the end of contrast injection and the initiation of the 3 sequential scan protocols. In a previous study, peak enhancement of the liver during pediatric CT was found to occur 3 to 12 s after initiation of contrast injection with a power injector.[56] In all 3 protocols, we found that image quality was sufficient for distinguishing ovarian margins from adnexa and for distinguishing antral follicles from stroma. The antral follicle margins were slightly less distinguishable in protocol 2 (100 mA, 0.8 s), and the ovary margins were slightly less distinguishable in protocol 3 (80 mA, 1.0 sec). Image noise (standard deviation of CT number) was the same for all 3 protocols in the left ovary but slightly lower for protocol 3 versus protocols 1 or 2 in the right ovary. It is possible that streak artifacts from pelvic bones and the metallic object in the colon could have affected ovarian image noise overall, regardless of the protocols.[59]

We used 2 methods to measure radiation dose delivered to the ovarian region during MDCT scanning in 2 of the monkeys. Here, we standardized the kVp (80), mA (100), and rotation time (0.5 s). We varied the slice thickness from 0.5 to 1 mm. TLDs were used to measure surface radiation exposure by using heat-stimulated emission of light after TLD irradiation.[35] With these detectors, the amount of emitted light is proportional to the total radiation dose received. CTDIs were used to estimate radiation exposure in light of ion chamber measurements of radiation dose obtained for the particular X-ray mAs (product of mA and rotation time) and kVp settings used during the scan. [29] Values reflected an average dose to the subject's volume, whereas TLD measurements reflected peripheral point dose at the surface. Radiation doses delivered to the ovarian region in our 2 monkeys were similar for the 2 protocols (corrected CTDI value, 0.6 rad each). This similarity indicates that slice thickness did not have a great effect on radiation dose. These radiation doses and the cumulative radiation dose from both scans (TLD value, 0.7 rad) were much lower than those previously reported

Table 4. Histologic follicle counts in macaques 7232 and 7235

	Primordial + intermediate	Primary	Secondary	Antral	Total
7232	1960	183	84	4	2231
7235	1419	57	24	3	1503

Table 5. MDCT volume, gross volume, MDCT antral follicle counts, and histologic antral follicle counts for ovaries in macaques 7232 and 7235

Protocol no.	4		5	
Macaque no.	7232	7235	7232	7235
MDCT volume (ml)[a]	0.67	0.54	0.66	0.41
Gross untrimmed volume, with adnexa (ml)	1.5	0.60	1.5	0.60
Gross trimmed volume (ml)	0.65	0.40	0.65	0.40
MDCT antral follicle count	3	5	5	5
Histologic antral follicle count	4	3	4	3

See Table 1 for protocol descriptions.
[a]Average of 3 measurements.

to cause ovarian damage in humans and macaques;[2,4,67] the LD50 of the human oocyte has been estimated to be 200 rad.[67] For developing macaque ovaries, X-ray exposures of 270 rad were necessary for complete elimination of follicles.[2] In prenatal rhesus macaque studies, the number of primordial follicles was unaffected by X-ray exposures less than 3000 rad.[4]

Immediate postscan histologic examinations of ovaries in the same 2 macaques confirmed that some focal areas of nonenhancement on MDCT images matched the locations of antral follicles. However, our estimated antral follicle counts from MDCT were not the same as actual antral follicle counts from histology. MDCT may have overestimated follicle numbers because of image noise. Conversely, histology may have underestimated follicle numbers because of insufficient sampling. In future studies, perhaps stereology will be a useful tool for more definitively measuring MDCT follicle count accuracy.[11]

Ovarian volume estimates from 3 of 4 MDCT scans in 2 macaques were within 0.01 to 0.02 ml (0.02% to 0.03%) of trimmed ovarian volumes measured by water displacement. These MDCT estimates are closer than those previously reported in a study of granulosa cell tumors in women,[38] in which CT volumes of tumors were within 0.6% of actual tumor volumes. We set the window display level at the mean, midslice ovarian CT density value prior to performing our ovarian volume calculations. We chose this technique because a previous study found that this helps to maximize visualization of margins and accuracy of region of interest cursor placement.[65] An unexpected finding was the larger difference between MDCT and actual ovarian volumes measured from 0.5-mm thick CT slices (0.14 ml difference) versus 1 mm CT slices (0.01 ml difference) in macaque 7235. This result was primarily due to difficulties in distinguishing cranial and caudal ovarian margins from adnexa with the thinner slices. With the thinner slices, changes in cranial and caudal ovarian contour appeared to gradually blend in with surrounding adnexa. With the thicker slices, changes in cranial and caudal ovarian contour appeared more abrupt and increased observer certainty for placement of the volume ROIs. This finding is consistent with a previous study in which visual recognition of object boundaries was a greater source of CT volume inaccuracies than patient-related factors.[10]

In summary, our findings indicate that MDCT is a promising technique for serial in vivo characterization of ovarian morphology in longitudinal studies using monkeys. Scan data were collected from subjects in less than 30 s, with resulting views that made possible consistent identification of ovaries without interference from surrounding pelvic canal structures. Moreover, contrast-enhanced, pediatric MDCT protocols provided sufficient image quality for distinguishing ovarian margins and antral follicles while maintaining pelvic radiation doses below those previously reported to cause ovarian damage in women and macaques. Finally, ovarian volume estimates from MDCT scans closely matched values measured during postmortem examinations, an outcome that supports the utility of MDCT for longitudinal studies of ovarian morphology. Future studies with larger numbers of subjects are needed to confirm whether MDCT is sufficiently sensitive to detect the changes in ovarian morphology known to accompany the follicular depletion and hormonal irregularity indicative of the menopausal transition.

Acknowledgments

We thank Debra Fuller, RT, R, M, MR; J Jeffery Carr, MD, MSCE, FACC; Joshua C Tan; and Patricia J Christian, BSc, for their contributions to this study. This project was funded by R24 grant RR 022191 from the National Center for Research Resources and R01 grant AG 027847 from the National Center for Aging, National Institutes of Health.

References

1. **Abel TW, Voytko ML, Rance NE.** 1999. The effects of hormone replacement therapy on hypothalamic neuropeptide gene expression in a primate model of menopause. J Clin Endocrinol Metab **84:**2111–2118.
2. **Andersen AC, Nelson VG, Simpson ME.** 1972. Fractionated X-radiation damage to developing monkey ovaries. J Med Primatol **1:**318–325.
3. **Appt SE, Kaplan JR, Clarkson TB, Cline JM, Christian PJ, Hoyer PB.** 2006. Destruction of primordial ovarian follicles in adult cynomolgus macaques after exposure to 4-vinylcyclohexene diepoxide: a nonhuman primate model of the menopausal transition. Fertil Steril **86(Suppl 4):**1210–1216.
4. **Baker TG.** 1966.The sensitivity of oocytes in post-natal rhesus monkeys to x-irradiation. J Reprod Fertil **12:**183–192.
5. **Bastos CA, Oppermann K, Fuchs SC, Donato GB, Spritzer PM.** 2006. Determinants of ovarian volume in pre-, menopausal transition, and post-menopausal women: a population-based study. Maturitas **53:**405–412.
6. **Baxter BS, Sorenson JA.** 1981.Factors affecting the measurement of size and CT number in computed tomography. Invest Radiol **16:**337–341.
7. **Bazot M, Deligne L, Boudghene F, Buy JN, Lassau JP, Bigot JM.** 1999. Correlation between computed tomography and gross anatomy of the suspensory ligament of the ovary. Surg Radiol Anat **21:**341–346.

8. **Bellino FL, Wise PM.** 2003.Nonhuman primate models of menopause workshop. Biol Reprod **68:**10–18.
9. **Black A, Tilmont EM, Handy AM, Scott WW, Shapses SA, Ingram DK, Roth GS, Lane MA.** 2001. A nonhuman primate model of age-related bone loss: a longitudinal study in male and premenopausal female rhesus monkeys. Bone **28:**295–302.
10. **Breiman RS, Beck JW, Korobkin M, Glenny R, Akwari OE, Heaston DK, Moore AV, Ram PC.** 1982. Volume determinations using computed tomography. AJR Am J Roentgenol **138:**329–333.
11. **Charleston JS, Hansen KR, Thyer AC, Charleston LB, Gougeon A, Siebert JR, Soules MR, Klein NA.** 2007. Estimating human ovarian non-growing follicle number: the application of modern stereology techniques to an old problem. Hum Reprod **22:**2103–2110.
12. **Clarkson TB.** 1994. Estrogens, progestins, and coronary heart disease in cynomolgus monkeys. Fertil Steril **62:**147S–151S.
13. **Clarkson TB, Anthony MS, Klein KP.** 1994. Effects of estrogen treatment on arterial wall structure and function. Drugs **47 Suppl 2:**42–51.
14. **Cody DD, Moxley DM, Krugh KT, O'Daniel JC, Wagner LK, Eftekhari F.** 2004. Strategies for formulating appropriate MDCT techniques when imaging the chest, abdomen, and pelvis in pediatric patients. AJR Am J Roentgenol **182:**849–859.
15. **Colman RJ, Kemnitz JW, Lane MA, Abbott DH, Binkley N.** 1999. Skeletal effects of aging and menopausal status in female rhesus macaques. J Clin Endocrinol Metab **84:**4144–4148.
16. **Downs JL, Urbanski HF.** 2006. Neuroendocrine changes in the aging reproductive axis of female rhesus macaques (*Macaca mulatta*). Biol Reprod **75:**539–546.
17. **Eber J, Villasenor C.** 1991. Ultrasound: advantages, disadvantages, and controversies. Nurse Pract Forum **2:**239–242.
18. **Erdem M, Erdem A, Biberoglu K, Arslan M.** 2003. Age-related changes in ovarian volume, antral follicle counts and basal follicle stimulating hormone levels: comparison between fertile and infertile women. Gynecol Endocrinol **17:**199–205.
19. **Fearon T, Vucich J.** 1985. Pediatric patient exposures from CT examinations: GE CT/T 9800 scanner. AJR Am J Roentgenol **144:**805–809.
20. **Flaws JA, Doerr JK, Sipes IG, Hoyer PB.** 1994. Destruction of preantral follicles in adult rats by 4-vinyl-1-cyclohexene diepoxide. Reprod Toxicol **8:**509–514.
21. **Flaws JA, Langenberg P, Babus JK, Hirshfield AN, Sharara FI.** 2001. Ovarian volume and antral follicle counts as indicators of menopausal status. Menopause **8:**175–180.
22. **Foshager MC, Walsh JW.** 1994. CT anatomy of the female pelvis: a second look. Radiographics **14:**51–64; discussion 64–56.
23. **Frush DP.** 2002. Pediatric CT: practical approach to diminish the radiation dose. Pediatr Radiol **32:**714–717; discussion 751–714.
24. **Frush DP, Donnelly LF, Bisset GS, 3rd.** 2001. Effect of scan delay on hepatic enhancement for pediatric abdominal multislice helical CT. AJR Am J Roentgenol **176:**1559–1561.
25. **Giacobbe M, Mendes Pinto-Neto A, Simoes Costa-Paiva LH, Martinez EZ.** 2004. The usefulness of ovarian volume, antral follicle count and age as predictors of menopausal status. Climacteric **7:**255–260.
26. **Gilardi KV, Shideler SE, Valverde CR, Roberts JA, Lasley BL.** 1997. Characterization of the onset of menopause in the rhesus macaque. Biol Reprod **57:**335–340.
27. **Goswamy RK, Campbell S, Royston JP, Bhan V, Battersby RH, Hall VJ, Whitehead MI, Collins WP.** 1988. Ovarian size in postmenopausal women. Br J Obstet Gynaecol **95:**795–801.
28. **Hormann M, Philipp MO, Eberl H, Windberger U, Matzek W, Schafer-Prokop C, Metz VM.** 2004. The effect of varying low-dose protocols on perceived image quality in multidetector CT in a rabbit model of acute appendicitis. Eur Radiol **14:**1465–1471.
29. **Horton KM, Sheth S, Corl F, Fishman EK.** 2002. Multidetector row CT: principles and clinical applications. Crit Rev Comput Tomogr **43:**143–181.
30. **Hutz RJ, Dierschke DJ, Wolf RC.** 1986. Markers of atresia in ovarian follicular components from rhesus monkeys treated with estradiol-17 beta. Biol Reprod **34:**65–70.
31. **Judy PF, Swensson RG, Szulc M.** 1981. Lesion detection and signal-to-noise ratio in CT images. Med Phys **8:**13–23.
32. **Kaplan JR, Adams MR, Clarkson TB, Manuck SB, Shively CA.** 1991. Social behavior and gender in biomedical investigations using monkeys: studies in atherogenesis. Lab Anim Sci **41:**334–343.
33. **Krajewski SJ, Abel TW, Voytko ML, Rance NE.** 2003. Ovarian steroids differentially modulate the gene expression of gonadotropin-releasing hormone neuronal subtypes in the ovariectomized cynomolgus monkey. J Clin Endocrinol Metab **88:**655–662.
34. **Kritzer MF, Adler A, Bethea CL.** 2003. Ovarian hormone influences on the density of immunoreactivity for tyrosine hydroxylase and serotonin in the primate corpus striatum. Neuroscience **122:**757–772.
35. **Kron T, Elliot A, Wong T, Showell G, Clubb B, Metcalfe P.** 1993. X-ray surface dose measurements using TLD extrapolation. Med Phys **20:**703–711.
36. **Kumar P, Rehani MM, Kumar L, Sharma R, Bhatla N, Singh R, Sundaram KR.** 2002. Potential of CT-scan based tumor volume as a response indicator in chemotherapy of advanced epithelial ovarian cancer. Med Sci Monit **8:**CR667–674.
37. **Lass A, Skull J, McVeigh E, Margara R, Winston RM.** 1997. Measurement of ovarian volume by transvaginal sonography before ovulation induction with human menopausal gonadotrophin for in-vitro fertilization can predict poor response. Hum Reprod **12:**294–297.
38. **MacSweeney JE, King DM.** 1994. Computed tomography, diagnosis, staging and follow-up of pure granulosa cell tumour of the ovary. Clin Radiol **49:**241–245.
39. **Mann DR, Gould KG, Collins DC.** 1990. A potential primate model for bone loss resulting from medical oophorectomy or menopause. J Clin Endocrinol Metab **71:**105–110.
40. **Mayer LP, Devine PJ, Dyer CA, Hoyer PB.** 2004. The follicle-deplete mouse ovary produces androgen. Biol Reprod **71:**130–138.
41. **Mukherji SK, Toledano AY, Beldon C, Schmalfuss IM, Cooper JS, Sicks JD, Amdur R, Sailer S, Loevner LA, Kousouboris P, Ang K.** 2005. Interobserver reliability of computed tomography-derived primary tumor volume measurement in patients with supraglottic carcinoma. Cancer **103:**2616–2622.
42. **Nawaratne S, Fabiny R, Brien JE, Zalcberg J, Cosolo W, Whan A, Morgan DJ.** 1997. Accuracy of volume measurement using helical CT. J Comput Assist Tomogr **21:**481–486.
43. **Nelson LH, Kremkau FW.** 1991. Introduction to transvaginal imaging. Obstet Gynecol Clin North Am **18:**683–692.
44. **Nichols SM, Bavister BD, Brenner CA, Didier PJ, Harrison RM, Kubisch HM.** 2005. Ovarian senescence in the rhesus monkey (*Macaca mulatta*). Hum Reprod **20:**79–83.
45. **Occhipinti KA, Frankel SD, Hricak H.** 1993. The ovary. Computed tomography and magnetic resonance imaging. Radiol Clin North Am **31:**1115–1132.
46. **Oppermann K, Fuchs SC, Spritzer PM.** 2003. Ovarian volume in pre- and perimenopausal women: a population-based study. Menopause **10:**209–213.
47. **Pavlik EJ, DePriest PD, Gallion HH, Ueland FR, Reedy MB, Kryscio RJ, van Nagell JR, Jr.** 2000. Ovarian volume related to age. Gynecol Oncol **77:**410–412.
48. **Pedersen T, Peters H.** 1968. Proposal for a classification of oocytes and follicles in the mouse ovary. J Reprod Fertil **17:**555–557.
49. **Rapp PR, Morrison JH, Roberts JA.** 2003. Cyclic estrogen replacement improves cognitive function in aged ovariectomized rhesus monkeys. J Neurosci **23:**5708–5714.
50. **Rebner M, Gross BH, Korobkin M, Ruiz J.** 1989. CT appearance of right gonadal vein. J Comput Assist Tomogr **13:**460–462.
51. **Register TC, Wagner JD, Zhang L, Hall J, Clarkson TB.** 2002. Effects of tibolone and conventional hormone replacement therapies on arterial and hepatic cholesterol accumulation and on circulating endothelin-1, vascular cell adhesion molecule-1, and E-selectin in surgically menopausal monkeys. Menopause **9:**411–421.
52. **Rigsby CK, Siegel MJ.** 1994. CT appearance of pediatric ovaries and uterus. J Comput Assist Tomogr **18:**72–76.
53. **Roberts JA, Gilardi KV, Lasley B, Rapp PR.** 1997. Reproductive senescence predicts cognitive decline in aged female monkeys. Neuroreport **8:**2047–2051.

54. **Robinson D, Rainer RO, Washburn SA, Clarkson TB.** 1996. Effects of estrogen and progestin replacement on the urogenital tract of the ovariectomized cynomolgus monkey. Neurourol Urodyn **15:**215–221.
55. **Rozenblit AM, Ricci ZJ, Tuvia J, Amis ES, Jr.** 2001. Incompetent and dilated ovarian veins: a common CT finding in asymptomatic parous women. AJR Am J Roentgenol **176:**119–122.
56. **Ruess L, Bulas DI, Kushner DC, Silverman PM, Fearon TC.** 1998. Peak enhancement of the liver in children using power injection and helical CT. AJR Am J Roentgenol **170:**677–681.
57. **Saksouk FA, Johnson SC.** 2004. Recognition of the ovaries and ovarian origin of pelvic masses with CT. Radiographics **24(Suppl 1):**S133–146.
58. **Siegel MJ, Schmidt B, Bradley D, Suess C, Hildebolt C.** 2004. Radiation dose and image quality in pediatric CT: effect of technical factors and phantom size and shape. Radiology **233:**515–522.
59. **Solomon SL, Jost RG, Glazer HS, Sagel SS, Anderson DJ, Molina PL.** 1991. Artifacts in computed radiography. AJR Am J Roentgenol **157:**181–185.
60. **Stroud FC, Appt SE, Wilson ME, Franke AA, Adams MR, Kaplan JR.** 2006. Concentrations of isoflavones in macaques consuming standard laboratory monkey diet. J Am Assoc Lab Anim Sci **45:**20–23.
61. **Suess C, Chen X.** 2002. Dose optimization in pediatric CT: current technology and future innovations. Pediatr Radiol **32:**729–734; discussion 751–724.
62. **Szebenyi ES.** 1969. Atlas of macaca mulatta. Cranbury, NJ: Associated University Presses.
63. **Tepper R, Zalel Y, Markov S, Cohen I, Beyth Y.** 1995. Ovarian volume in postmenopausal women—suggestions to an ovarian size nomogram for menopausal age. Acta Obstet Gynecol Scand **74:**208–211.
64. **Tiitola M, Vehmas T, Kivisaari RP, Kivisaari L.** 1997. Optimising imaging parameters in experimental spiral CT. Acta Radiol **38:**913–917.
65. **Ullrich CG, Binet EF, Sanecki MG, Kieffer SA.** 1980. Quantitative assessment of the lumbar spinal canal by computed tomography. Radiology **134:**137–143.
66. **Verdun FR, Lepori D, Monnin P, Valley JF, Schnyder P, Gudinchet F.** 2004. Management of patient dose and image noise in routine pediatric CT abdominal examinations. Eur Radiol **14:**835–841.
67. **Wallace WH, Thomson AB, Kelsey TW.** 2003. The radiosensitivity of the human oocyte. Hum Reprod **18:**117–121.